The Use of TVD Limiters for Forward-in-Time Upstream-Biased Advection Schemes in Ocean Modeling

JULIE PIETRZAK

Danish Meteorological Institute, Copenhagen, Denmark, and
International Research Center for Computational Hydrodynamics, Horsholm, Denmark

(Manuscript received 15 July 1996, in final form 4 August 1997)

ABSTRACT

This paper explores the use of the constant grid flux form forward-in-time upstream-biased advection schemes for the advection of temperature and salinity in ocean modeling. The constant grid flux form schemes are shown to be an improvement over the traditional central differencing commonly used in ocean models. In addition, nonoscillatory versions of the scheme, which employ flux limiters, are explored. The limiters are based on total variation diminishing concepts and are applied to higher-order (in space) versions of the constant grid flux form scheme. The constant grid flux form schemes are Crowley-type upstream-biased Eulerian advection schemes. They are mass conserving and possess small amplitude and phase errors. The flux limiters prevent the under- and overshooting associated with the numerical dispersion of the unlimited schemes. The limited schemes are easy to implement, efficient, and nonoscillatory. Of these schemes the third-order and fifth-order versions employing the PDM limiter are shown to give optimal results for the advection of scalars under a number of test cases. There is a trade-off between the greater accuracy of the fifth-order scheme and the requirement of a larger grid stencil associated with a greater computational cost. Higher-order nonoscillatory schemes can easily be developed for three-dimensional primitive equation modeling. A multidimensional version is presented that employs a modified time-splitting technique. It is shown to be suitable for three-dimensional primitive equation modeling.

1. Introduction

A three-dimensional version of a forward-in-time advection scheme based on the work of Leonard (1991), Easter (1993), and Hundsdorfer and Trompert (1994) is discussed in this paper that combines the Crowley schemes (Leith 1965; Crowley 1968; Tremback et al. 1987) with limiters based on total variation diminishing concepts. Harten (1983, 1984) introduced total variation diminishing (TVD) concepts to characterize oscillation-free schemes. These concepts are an important contribution to modern high-resolution advection schemes. These schemes, which are described in detail in Hirsch (1990) and LeVeque (1992), are at least second-order accurate on smooth solutions and yet give well-resolved, nonoscillatory discontinuities. Zalesak (1987) compared a number of high-resolution schemes, dividing them into geometric schemes (Godunov) and algebraic schemes that employ flux limiters to enforce some constraint on the solution, usually the TVD property.

High-resolution schemes, employing some form of limiter, are routinely used in a wide range of engineering problems, particularly in aerodynamics, however, they have not gained widespread acceptance in either the meteorological or oceanographic communities. They were generally thought to be too complicated and too time consuming for use in solving the advection terms in three-dimensional primitive equation models. Only recently have these concepts been introduced into meteorological modeling, for example, Carpenter et al. (1990), Xue and Thorpe (1991), Lin et al. (1994), and Lin and Rood (1996) have found that the Gudonov schemes, monotonic upstream centered schemes for conservation laws (MUSCL) (van Leer 1977, 1979), and its higher-order variant, the piecewise parabolic method (PPM) (Collella and Woodward 1984), can successfully model mesoscale and global problems. Alternatively flux-limited forward-in-time schemes have been used successfully by Thuburn (1993) for vertical advection in a global circulation model and by Hundsdorfer and Spee (1995) for atmospheric modeling of global transport of constituents.

Recently James (1996) in a comparison of advection schemes suitable for shelf sea modeling, recommended the PPM scheme over a TVD version of the Lax–Wendroff scheme. However, Hundsdorfer and Trompert (1994) introduced a flux-limited, third-order (in space) forward-in-time upstream-biased advection scheme. Their scheme gave good results in a two-dimensional

Corresponding author address: Dr. Julie D. Pietrzak, International Research Center for Computational Hydrodynamics, Agern Alle 5, DK-2970 Hørsholm, Denmark.

© 1998 American Meteorological Society

simulation of a front. Instead of the Superbee limiter used with the Lax–Wendroff scheme (Lax and Wendroff 1964) they used a limiter similar to the PDM limiter described in the review by Zalesak (1987). In the following a number of flux limiters are compared and it is shown that higher-order nonoscillatory schemes can easily be developed that are suitable for three-dimensional primitive equation modeling. While attention is paid to the third-order version the method can easily be extended to higher orders and is therefore more general than the van Leer and PPM method.

Forward-in-time upstream-biased schemes have a long history in meteorology and were adopted as higher-order methods to limit both the numerical diffusion of the low-order upstream scheme and the numerical dispersion associated with the central leapfrog scheme. The leapfrog scheme was widely adopted for large-scale simulations in both meteorology and oceanography because of its simplicity and computational efficiency. Lilly (1965) and Arakawa (1966) also considered its lack of amplitude errors to be more important than its dispersion errors in long-term integrations. However, in regions where large gradients exist these errors can corrupt the flow with dispersive ripples. In order to overcome these problems higher-order schemes have been developed to minimize both numerical diffusion and numerical dispersion. Leith (1965) and Crowley (1968) used the upstream method combined with polynomial fitting to construct higher-order accurate advection schemes. This method was extended to arbitrary ordered polynomials by Tremback et al. (1987). They compared a number of methods for fitting polynomials and concluded that the best results were obtained with the constant grid flux form (CGF) method. It is worth noting that in the case of constant grid spacing, the second-order polynomial CGF scheme is the same as the QUICKEST (quadratic upstream interpolation for convective kinematics with estimated stream terms) scheme (Leonard 1979). While these schemes are less diffusive than simple upstream schemes, all higher-order advection schemes suffer from numerical dispersion, which leads to the generation of negative values in solutions for positive definite functions Hirsch (1990).

In an attempt to overcome this problem with a minimal increase in computational cost, positive definite schemes have recently been used in meteorological models. Bott (1989a,b) developed a positive definite scheme, which is a generalization of the constant grid flux form, by introducing area-preserving polynomials and a positive definite limitation procedure. In contrast, Smolarkiewicz (1983, 1984) and Smolarkiewicz and Clark (1986) developed a conservative and positive definite scheme using an iterative approach. By introducing corrective advective fluxes the truncation error caused by the upstream method is significantly reduced. Both of these schemes have found widespread use in the meteorological community and have been employed in the advection of humidity and cloud water in realistic three-dimensional weather simulations by Berge and Kristjansson (1992).

More recently, monotonicity-preserving or shape-preserving upstream biased schemes have received greater attention. Of these the flux-corrected transport scheme (FCT) (Boris and Book 1976; Zalesak 1979) has gained widespread acceptance. This is essentially a two-step method in which a transport step is taken followed by an antidiffusive correction. Smolarkiewicz and Grabowski (1990) introduced monotonicity limiters of the FCT type. Whereas the FCT method has been widely adopted in both meteorology and oceanography, the application of TVD methods is rather limited. The sufficient conditions defining TVD schemes are described in detail in Hirsch (1990) and LeVeque (1992). They can be constructed either by flux or slope-limiter methods. Sweby (1984) studied a wide range of flux-limiter methods and derived conditions on the limiter function that guaranteed second-order accuracy and the TVD property. In order to assess the performance of TVD flux limiters on an upstream biased advection scheme, the constant grid flux form scheme of Tremback et. al (1987) was selected. This is because this scheme has lower dispersion errors than the flux form scheme derived by fitting a polynomial exactly to each value of the scalar within a grid cell.

In the following, nonoscillatory versions of the constant grid flux form scheme are compared. In particular the PDM limiter is found to give the best overall results for a number of classic one- and two-dimensional test cases. A three-dimensional extension of the scheme is then described. The extension to three-dimensional flows uses a technique based on the work of Easter (1993). Either Strang splitting or a corrected velocity field method (Hundsdorfer and Trompert 1994) can be used to maintain a second-order accurate scheme in nonuniform flow fields. The present study is motivated by the need to investigate and improve the advection of fields with sharp gradients in numerical ocean modeling. Many of the three-dimensional primitive equation ocean models in widespread use still employ the leapfrog scheme. As one example of this, the Princeton Ocean Model [POM; Blumberg and Mellor (1987)] has been used in a wide range of simulations, ranging from estuarine to basin scale. It is well known that numerical dispersion can be a problem, for example, in frontal regions where large gradients of temperature and salinity exist. The POM model is used in the three-dimensional primitive experiments described in this paper.

While the classic one- and two-dimensional examples highlight the performance of the different limiters in simple test cases, it is unclear whether these schemes will give the same improvements in the simulation of more realistic three-dimensional flows. Very few papers in oceanography have addressed this situation. One of the notable exceptions is the work of James (1996). His work is extended in this paper by considering higher-order (in space) schemes and alternative TVD limiters.

The leapfrog scheme was adopted as the scheme of choice in numerical ocean modeling because it is simple to implement, has no numerical damping, and conserves quadratic quantities. However, on scales of the order of the internal Rossby radius of deformation, the interest of many modelers is to resolve the flow in regions where strong gradients exist. It is precisely these small-scale features such as occur at fronts, hydraulic jumps, and upwelling regions that one wishes to resolve in coastal ocean modeling. The large spatial gradients of salinity and temperature that can occur in such regions place strong constraints on the numerical model.

Therefore consideration is given in this paper to flows in frontal regions, with particular emphasis on estuarine flow situations, such as occur in the waters connecting the salty North Sea with the brackish Baltic Sea. Section 2 describes the Crowley-type advection schemes and their TVD formulation. In section 3 the effect of different limiters is explored and analyzed in detail. Finally in section 4 the suitability of the schemes for three-dimensional ocean modeling is discussed and conclusions are presented.

2. Theory

a. Forward-in-time upstream differencing

The advection equation describing the transport of a nondiffusive quantity $\psi(x, y, z, t)$ in a nondivergent flow field is given by

$$\frac{\partial \psi}{\partial t} = -\nabla \cdot (\mathbf{v}\psi), \tag{1}$$

where for example ψ is a scalar quantity, a tracer mixing ratio, or temperature and salinity in the primitive equation applications; $\mathbf{v}$ is the velocity vector; (x, y, z) is a position vector in a Cartesian coordinate system; and t is time. For simplicity the one-dimensional case is considered in this section. The discrete forward-in-time upstream solution of Eq. (1), on a staggered grid, can be written as

$$\psi_j^{n+1} = \psi_j^n - \frac{\Delta t}{\Delta x}(F_{j+1/2}^n - F_{j-1/2}^n), \tag{2}$$

where ψ_j^n is the value of ψ at grid point j after n time steps, $F_{j+1/2}^n$, $F_{j-1/2}^n$ are the ψ fluxes through the right and left boundaries of the grid box, and Δx and Δt are the grid spacing and time step, respectively. The flux through the right boundary can be found from

$$F_{j+1/2}^n = \frac{1}{\Delta t}\int_{x_{j+1/2}-u\Delta t}^{x_{j+1/2}} \psi(x')\, dx', \tag{3}$$

and these schemes are referred to as upstream schemes in the sense that they interpolate a distance $x' = (x_{j+1/2} - u\Delta t)$ upstream. It is worth noting that the departure point x' in the schemes' derivation assumes a constant velocity in space and time. The distribution of ψ within each grid box j is approximated by a polynomial of order ℓ,

$$\psi_{j,1}^n(x') = \sum_{k=0}^{\ell} a_{j,k}^n \left(\frac{x - x_j}{\Delta x_j}\right)^k, \tag{4}$$

where the coefficients $a_{j,k}$ are functions of $(\ell + 1)\psi$ values. Following the CGF philosophy, the coefficients are determined by solving

$$\psi_i^n \Delta x_i = \int_{x_{i-1/2}'}^{x_{i+1/2}'} \sum_{k=0}^{\ell} a_{j,k}^n \left(\frac{x - x_j}{\Delta x_j}\right)^k dx' \tag{5}$$

with $i = j, j \pm 1, j \pm 2, \ldots$. Therefore, the coefficients for nonuniform grids can easily be calculated. The coefficients for a uniform grid are listed in Bott (1989b) for $\ell = 2$ and $\ell = 4$ and are the same as those described by Tremback et al. (1987) for their constant grid flux form. Additionally, the $\ell = 2$ coefficients are the same as those described by Leonard (1979) and used by Hundsdorfer and Trompert (1994) as the basis for their third-order-in-space schemes. The fluxes are easily found by evaluating the integral in Eq. (3). It is worth noting that the even-order, second- and fourth-order polynomial versions (P2 and P4) discussed here refer to third- and fifth-order accurate (in space) schemes, respectively.

In order to highlight the hybrid nature of the limited schemes, to be described in the following section, the fluxes can be written as a first-order upstream contribution and a higher-order correction term. Using the P2 scheme as an example, the positive and negative fluxes corresponding to $c_{j+1/2}^+ = \max(0, c_{j+1/2}^n)$ and $c_{j+1/2}^- = \min(c_{j+1/2}^n, 0)$, where $c_{j\pm1/2}^{\pm}$ is the Courant number, can be written

$$F_{j+1/2}^+ = c_{j+1/2}^+ \frac{\Delta t}{\Delta x}\left\{\psi_j^n + \frac{1}{2}(1 - |c_{j+1/2}|) \times [\alpha(\psi_{j+1}^n - \psi_j^n) + \beta(\psi_j^n - \psi_{j-1}^n)]\right\} \tag{6}$$

$$F_{j+1/2}^- = c_{j+1/2}^- \frac{\Delta t}{\Delta x}\left\{\psi_{j+1}^n - \frac{1}{2}(1 - |c_{j+1/2}|) \times [\alpha(\psi_{j+1}^n - \psi_j^n) + \beta(\psi_{j+2}^n - \psi_{j+1}^n)]\right\} \tag{7}$$

with $\alpha = [(1/2) + (1/6)(1 - 2|c_{j+1/2}^n|)]$, $\beta = [(1/2) - (1/6)(1 - 2|c_{j+1/2}^n|)]$, respectively.

b. Total variation diminishing limiters

Harten (1983) introduced the concept of total variation diminishing schemes and slope limiter methods. These concepts were originally introduced to solve sca-

lar conservation laws and have been successfully applied to the Euler and Navier–Stokes equations. The importance of these schemes lies in the fact that all TVD schemes are monotonicity preserving. This simply means that monotone profiles are preserved during the time evolution and no new under- or overshoots are created. Defining the total variation as

$$\mathrm{TV}(\psi^n) = \sum_j \left|\psi^n_{j+1} - \psi^n_j\right| \tag{8}$$

the TVD constraints are satisfied if

$$\mathrm{TV}(\psi^{n+1}) \le \mathrm{TV}(\psi^n). \tag{9}$$

For example, if a scheme can be written in the general form,

$$\psi^{n+1}_j = \psi^n_j - B^+_{j-1/2}(\psi^n_j - \psi^n_{j-1}) - B^-_{j+1/2}(\psi^n_{j+1} - \psi^n_j), \tag{10}$$

then the sufficient conditions for Eq. (10) to satisfy the TVD constraints are

$$B^+_{j+1/2} \ge 0, \qquad B^-_{j+1/2} \le 0 \tag{11}$$

$$B^+_{j+1/2} - B^-_{j+1/2} \le 1, \tag{12}$$

where $B^{\pm}$ may depend on ψ and c. A recipe for the construction of TVD schemes is to select an advection scheme, rewrite it in the form of Eq. (10), and modify it so that the TVD constraints Eqs. (11) and (12) are satisfied.

Zalesak (1987) used this methodology to obtain high-order flux-limited schemes. He generalized the Φ flux limiter concept of Sweby (1984) by introducing the concepts of target high-order fluxes and of normalization high-order fluxes. Introducing a flux limiter Φ, the flux $F_{j+1/2}$ can be written as,

$$F_{j+1/2} = F^L_{j+1/2} + \Phi_{j+1/2}(F^H_{j+1/2} - F^L_{j+1/2}) \tag{13}$$

and the target high-order flux, $F^T_{j+1/2}$, as

$$F^T_{j+1/2} = F^L_{j+1/2} + \Phi^T_{j+1/2}(F^H_{j+1/2} - F^L_{j+1/2}), \tag{14}$$

where $F^L_{j+1/2}$ is the first-order upstream flux and $F^H_{j+1/2}$ is a high-order flux. If $F^H_{j+1/2}$ is taken to be the target high-order flux, then $\Phi_{j+1/2}$ equal to 1 returns the desired high-order flux, $F_{j+1/2}$. If, however, $F^H_{j+1/2}$ serves to normalize $\Phi_{j+1/2}$ and the target flux is in fact another high-order flux, then $\Phi_{j+1/2}$ equal to 1 will give the normalization flux. The target high-order flux could be defined by Eqs. (6) and (7), for example. Zalesak (1987) used the Lax–Wendroff flux, $F^{LW}_{j+1/2}$ (equivalent to the P1 flux), as the normalizing flux. In addition he introduced the term normalization high-order target flux, $\phi^T_{j+1/2} = (F^T_{j+1/2} - F^L_{j+1/2})(F^{LW}_{j+1/2} - F^L_{j+1/2})^{-1}$. This simply represents the ratio of the high-order flux contribution to the Lax–Wendroff flux contribution. For example, taking a positive high-order CGF flux, as the target high-order flux and normalizing with the Lax–Wendroff flux, Eq. (13) can be rewritten as

$$F^+_{j+1/2} = c^+_{j+1/2}\frac{\Delta t}{\Delta x}\left\{\psi^n_j + \frac{1}{2}\Phi_{j+1/2}(1 - |c_{j+1/2}|)[(\psi^n_{j+1} - \psi^n_j)]\right\} \tag{15}$$

and a similar equation can be written for the negative fluxes. Equation (15) has the same form as the flux limited Lax–Wendroff scheme. The choice of limiter therefore determines Φ, and Eq. (13) can be used to calculate the flux. If the limiter $\Phi_{j+1/2}$ equals the normalization high-order target flux, $\phi^T_{j+1/2}$, the full high-order flux is recovered and if $\Phi_{j+1/2} = 1$ the Lax–Wendroff flux is recovered. If $\Phi_{j+1/2} = 0$ the upstream scheme is used. For example, in the case of the positive P2 scheme, $\phi^{T+}_{j+1/2} = \alpha + \beta r^{n+}_{j+1/2}$. As TVD concepts are expressed as a function of ratios of consecutive variations, the limiters can be defined as functions of these ratios. In the case of the CGF schemes the slope ratios defined by $r^{n+}_{j+1/2} = (\psi^n_j - \psi^n_{j-1})(\psi^n_{j+1} - \psi^n_j)^{-1}$ are employed. An equation of the form of Eq. (10) can easily be obtained by substituting Eq. (15) into Eq. (2). This gives

$$\psi^{n+1}_j = \psi^n_j - c(\psi^n_j - \psi^n_{j-1}) \times \left[1 + \frac{1}{2}(1 - c)\frac{\Phi_{j+1/2}}{r^{n+}_{j+1/2}} - \frac{1}{2}(1 - c)\Phi_{j-1/2}\right], \tag{16}$$

where for simplicity a constant positive velocity has been assumed, so that $B^-_{j+1/2} = 0$, and the subscripts and superscripts on c have been dropped temporarily. Therefore B^+ can be expressed as

$$B^+_{j-1/2} = c\left[1 + \frac{1}{2}(1 - c)\frac{\Phi_{j+1/2}}{r^{n+}_{j+1/2}} - \frac{1}{2}(1 - c)\Phi_{j-1/2}\right]. \tag{17}$$

The TVD constraints will be satisfied if

$$\Phi_{j-1/2} - \frac{\phi_{j+1/2}}{r^{n+}_{j+1/2}} \le \frac{2}{(1 - c)} \tag{18}$$

and

$$\frac{\Phi_{j+1/2}}{r^{n+}_{j+1/2}} - \Phi_{j-1/2} \le \frac{2}{c}. \tag{19}$$

It is also assumed that $\Phi_{j\pm1/2}$ is a positive function and that $\Phi_{j+1/2} = 0$ if $r^{n+}_{j+1/2} \le 0$. In addition $c \le 1$ is the CFL stability condition. A clear explanation of the TVD Lax–Wendroff scheme is given in the recent work by Thuburn (1997). He also includes the more general case of higher-order advection schemes, following Eq. (13), but in his example $F^H_{j+1/2}$ is the high-order target flux.

A number of limiter functions satisfy these constraints and are described in detail in Hirsch (1990) and LeVeque (1992). Zalesak (1987) reviewed a number of Sweby-type Φ limiter functions in widespread use, including the following:

minmod

$$\Phi(r) = \max[0, \min(1, r)],$$

van Leer monotonic

$$\Phi(r) = \max\{0, \min[(r + |r|)/(1 + r)]\},$$

MUSCL

$$\Phi(r) = \max\{0, \min[2, 2r, (1 + r)/2]\},$$

Superbee

$$\Phi(r) = \max[0, \min(1, 2r), \min(r, 2)], \quad \text{and}$$

arbitrary order PDM

$$\Phi(r) = \max\left[0, \min\left(\Phi^T, \frac{2}{1 - c}, \frac{2r}{c}\right)\right],$$

which are compared in the following. It is easy to see that limited advection schemes, of arbitrary order, can be written by a suitable definition of the ϕ^T terms. The PDM limiter defines the uppermost range of the TVD constraints. The PDM limiter can be applied to the higher-order advection schemes and in this sense it is referred to as arbitrary order. This is in contrast to the other limiters, for which no improvement would be found, as these limiters only depend on the ratio. Therefore the information about the underlying CGF schemes is now lost. Leonard (1991) acknowledges that the universal limiter, which was derived in a different manner, appears to be the equivalent of the PDM limiter. Zalesak (1987) attributed the PDM limiter to Lyon and Hain and showed that it could be successfully applied to higher-order schemes. This hybrid method uses the full flux in smooth regions and limits the solution near discontinuities, employing the monotone upwind method in these regions. If the limiter equals zero, then the upstream method is used and if the limiter equals ϕ^T then the higher-order scheme is employed. The PDM limiter is used for higher-order advection. In the case of a variable velocity, the limited fluxes are calculated using Eq. (15) for a positive flux, with a similar equation for the negative flux. The value of c, used in the PDM limiter, is therefore taken as $c^{\pm}_{i+1/2}$, depending on whether the positive or negative flux is calculated.

c. Multidimensional second-order-accurate schemes

If the flow field varies, the upstream biased advection schemes possess a first-order error that arises from the assumption of a constant velocity field in their derivation [Eq. (3)]. In order to eliminate this error a higher-order correction term can be used in the estimation of the departure point. A common method for obtaining a second-order-accurate formula is simply to retain the second-order term in the Taylor series expansion for the velocity in the individual one-dimensional directions. In addition it is well known that time splitting introduces a first-order temporal error and leads to the generation of weak numerical instabilities in multidimensional deformational flow fields (Petschek and Libersky 1975). However, two fairly simple methods by which this error can be reduced are Strang splitting [see LeVeque (1992) for a detailed discussion] or a modified velocity method in which corrections are made to the background flow field, (Hundsdorfer and Trompert 1994). Either procedure is easily extended to three dimensions (see appendix). It should be noted that in order to obtain a fully second-order-in-time scheme, the velocity modifications can be extended to include **v** at the $n + \frac{1}{2}$ time level, by either interpolation or extrapolation (Smolarkiewicz 1991). Alternatively, a predictor–corrector version of these schemes could be used. While these methods of achieving a second-order-accurate scheme reduce the time-splitting error, they do not preserve a constant (to machine precision); see for example Hecht et al. (1995) who describe these corrections for achieving second-order accuracy.

However, Easter (1993) described a method to reduce the time-splitting error by following an approach similar to Russell and Lerner (1981). This approach involves the solution of a tracer mixing ratio–type problem together with the solution of the continuity equation in each of the individual one-dimensional time-splitting steps. This method, in combination with Strang splitting was shown to preserve a constant. It can also be applied with the modified velocity method to obtain a second-order-accurate method. Interestingly, his method can easily be extended for the solution of the advection equations in a three-dimensional primitive equation numerical model, in our case the sigma coordinate model POM. His method is adopted in the three-dimensional implementations described in the following. The advection equation for temperature and salinity in POM is given by

$$\frac{\partial \psi D}{\partial t} = -\frac{\partial UD\psi}{\partial x} - \frac{\partial VD\psi}{\partial y} - \frac{\partial \omega D\psi}{\partial \sigma} \tag{20}$$

and the continuity equation by

$$\frac{\partial D}{\partial t} = -\frac{\partial UD}{\partial x} - \frac{\partial VD}{\partial y} - \frac{\partial \omega D}{\partial \sigma}, \tag{21}$$

where ψ is either temperature or salinity and D is the depth of the fluid, U and V are the horizontal velocities, and ω is the sigma coordinate, σ, vertical velocity $D\sigma/Dt$. It is worth noting that a different definition for the vertical velocity is used here [see Blumberg and Mellor (1987) for a detailed description]. In order to apply time splitting to Eq. (20), it is necessary to account for volume changes into or out of the individual grid cells during each of the one-dimensional advection steps. For example,

$$\frac{\partial \psi D}{\partial t} = -\frac{\partial UD\psi}{\partial x} \tag{22}$$

needs to be solved together with the corresponding time-split continuity equation

$$\frac{\partial D}{\partial t} = -\frac{\partial UD}{\partial x} \tag{23}$$

in order to account for the temporary decrease (increase) in volume of the cell due to divergence (convergence). The intermediate values of both ψ and D are then input into the y equation, and the resulting values from this intermediate step are then input into the vertical equation. The scheme can easily be shown to be conservative. The value of D at time step $n + 1$ is known before the solution of the advection equation for temperature and salinity. This value should be the same as the value of D obtained from the solution of the x, y, and z continuity equations if the scheme is to be mass conserving. Numerical results demonstrated that this is the case. Applying either Strang splitting or the modified velocity corrections, the schemes can be made to retain second-order accuracy. The computationally cheaper alternative of utilizing the modified velocity scheme uses averaging, because of the staggered C grid, to calculate the different velocity components used in Eqs. (A11)–(A13) and may not be strictly second-order accurate near land boundaries. This may not be a serious violation for many practical purposes. In addition, the transport equation may include nonadvective terms R, on the right-hand side of Eq. (20). The POM includes the horizontal and vertical diffusion terms, solving the horizontal diffusion with the Smagorinsky formulation and the vertical with a level-2.5 turbulence closure scheme (Mellor and Yamada 1982). In the examples presented, horizontal diffusion is neglected if the forward-in-time schemes are used, but vertical diffusion is solved as in the original model. A second-order-accurate scheme may be maintained following Smolarkiewicz (1991) by discretizing R and $\mathbf{v}$ at the $n + \frac{1}{2}$ time level.

It is worth noting that while the TVD property is lost in the case of a multidimensional flow field (Goodman and LeVeque 1985) the limiters can be shown to retain positivity (Hundsdorfer and Trompert 1994). The schemes are effectively monotonicity preserving and in addition are positive definite.

3. Numerical results

In the following, the performance of the flux limiters and their suitability for scalar advection in primitive equation modeling are assessed. Consequently a number of classic one-, two-, and three-dimensional test cases have been carried out, as have fully three-dimensional primitive equation tests. See Pietrzak (1995) for a more detailed description of the implementation in the sigma coordinate POM code as well as for a more extensive number of one-, two-, and three-dimensional test cases. Due to the large number of numerical test cases only a few are presented here. In addition, see Sweby (1984) and Leonard (1991) for more extensive one-dimensional tests than those described here.

The results obtained with limited versions of the third- and fifth-order spatial schemes are compared. Tremback et al. (1987) found that polynomials up to 6 gave improved performance, minimizing the amplitude and phase errors. The second- and fourth-order polynomial versions (P2 and P4) were adopted in order to restrict the stencil used in the three-dimensional primitive equation ocean model. The fact that this model must be able to handle land boundaries restricts the size of the grid stencil.

a. One-dimensional experiments

The first set of experiments consider one-dimensional advection of a tracer in a constant velocity field. In these test cases two simple functions are advected, a square and a semicircle, which are superimposed on a background value of 1.0. The calculations were all performed in a periodic domain of length 100 with $\Delta x = 1$ m, a constant velocity $u = 1.0$ m s^{-1}, and time steps Δt of 0.5 s yielding a Courant number of 0.5. The limiters described in section 2b are compared.

Figures 1 and 2 show the results for two one-dimensional advection experiments after six complete revolutions around the periodic domain. Figure 1 shows the advection of a square wave and Fig. 2 shows the advection of a semicircle. The analytical solutions are shown as well as the numerical results. This figure highlights the main characteristics of the TVD limited schemes. In addition, Tables 1a and 1b compare the results with respect to L_2 errors, maximum and minimum values, and CPU time relative to the upstream scheme (P0) after six complete revolutions. The L_2 error is defined by $L_2^2 = N^{-1} \Sigma (\psi_c - \psi_e)^2$, where ψ_c is the calculated and ψ_e is the exact solution, and N is the total number of grid points. The naming convention adopted in the following is simply related to the order of the polynomial and the limiter employed, for example, P2_PDM refers to the third-order-in-space scheme, which uses a second-order polynomial and the PDM limiter. The schemes are mass conserving. The central leapfrog scheme is also included in the comparison, as this is the scheme used in the original version of POM code. Further, A_H is the horizontal diffusion coefficient which is only included to damp the numerical dispersion. Under- and overshooting is evident in Figs. 1 and 2 and the extreme values in Tables 1a,b.

While both the unlimited and limited schemes have essentially the same phase and amplitude performance, only the flux-limited versions are monotone, preventing under- and overshoot and remaining positive definite. The limited schemes presented are computationally efficient and easy to implement. The Superbee limiter displays its well-known overcompressive characteristics. It

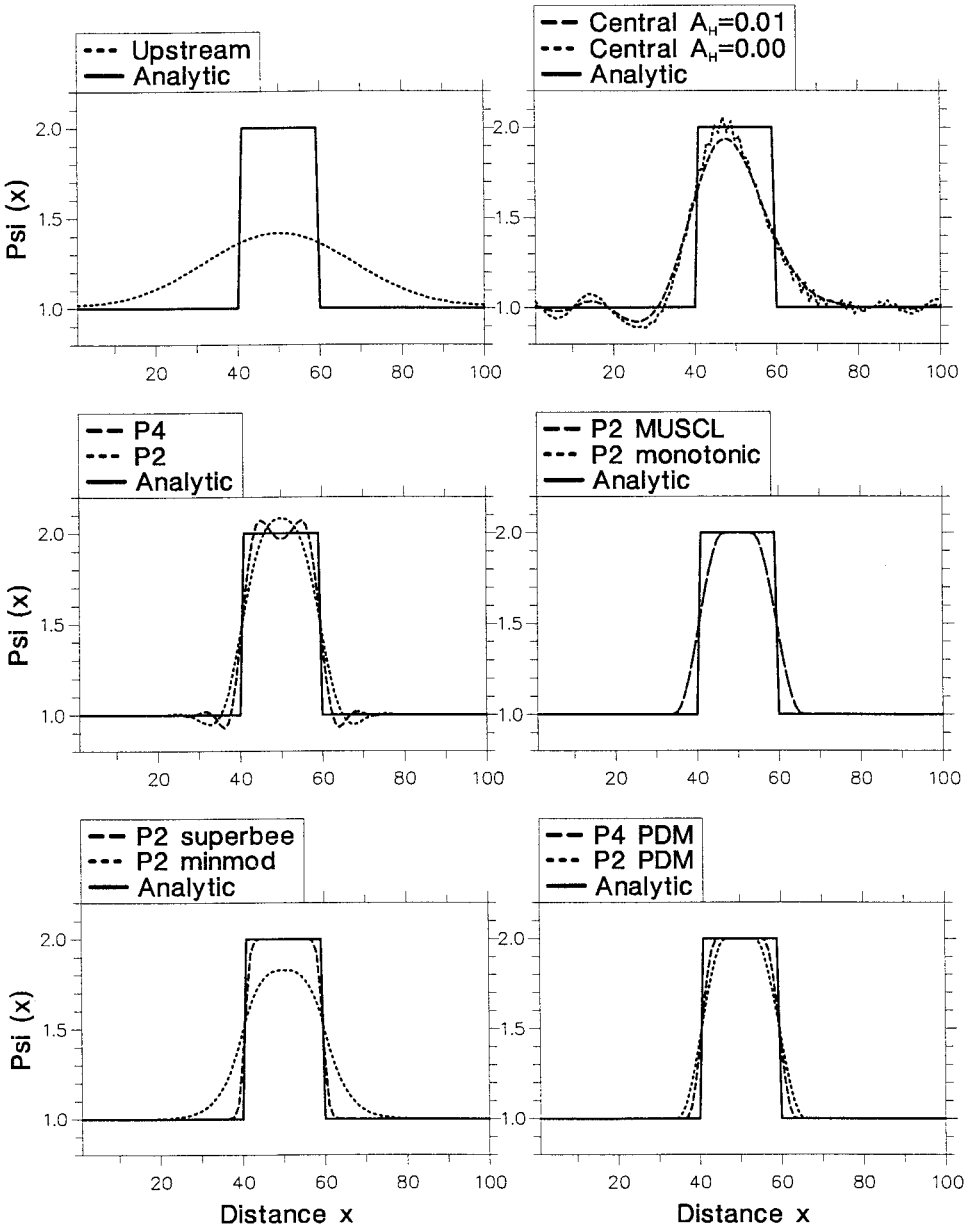

FIG. 1. A comparison of the advection schemes with the analytic solution showing the initial square and the numerical solution after six rotations through the domain.

handles discontinuities well but has a tendency to turn waves into squares. Some of the limiters give nearly identical results, for example, the monotonic and MUSCL, for the square wave test but their differences become apparent in the semicircle test. This is due to the dependence on the ratio in these limiters. In addition, a further test with a triangle (not shown) also supported the conclusion that the PDM limiter gives the best results for the 1D test cases. This is reflected both in the results summarized in Tables 1a,b, as well as in Figs. 1 and 2. The fifth-order scheme is more accurate, as expected. However, it requires more CPU time.

b. Two-dimensional advection experiments

To illustrate the behavior of the schemes in two dimensions a solid-body rotation test was chosen [Crowley 1968; Zalesak 1979; and Smolarkiewicz (1982)]. In these tests a prescribed distribution undergoes solid-body rotation counterclockwise around a 101 × 101 zone grid with $\Delta x = \Delta y = 1$. The velocity field is given by

$$u = -\omega(y - y_0)$$
$$v = \omega(x - x_0) \tag{24}$$

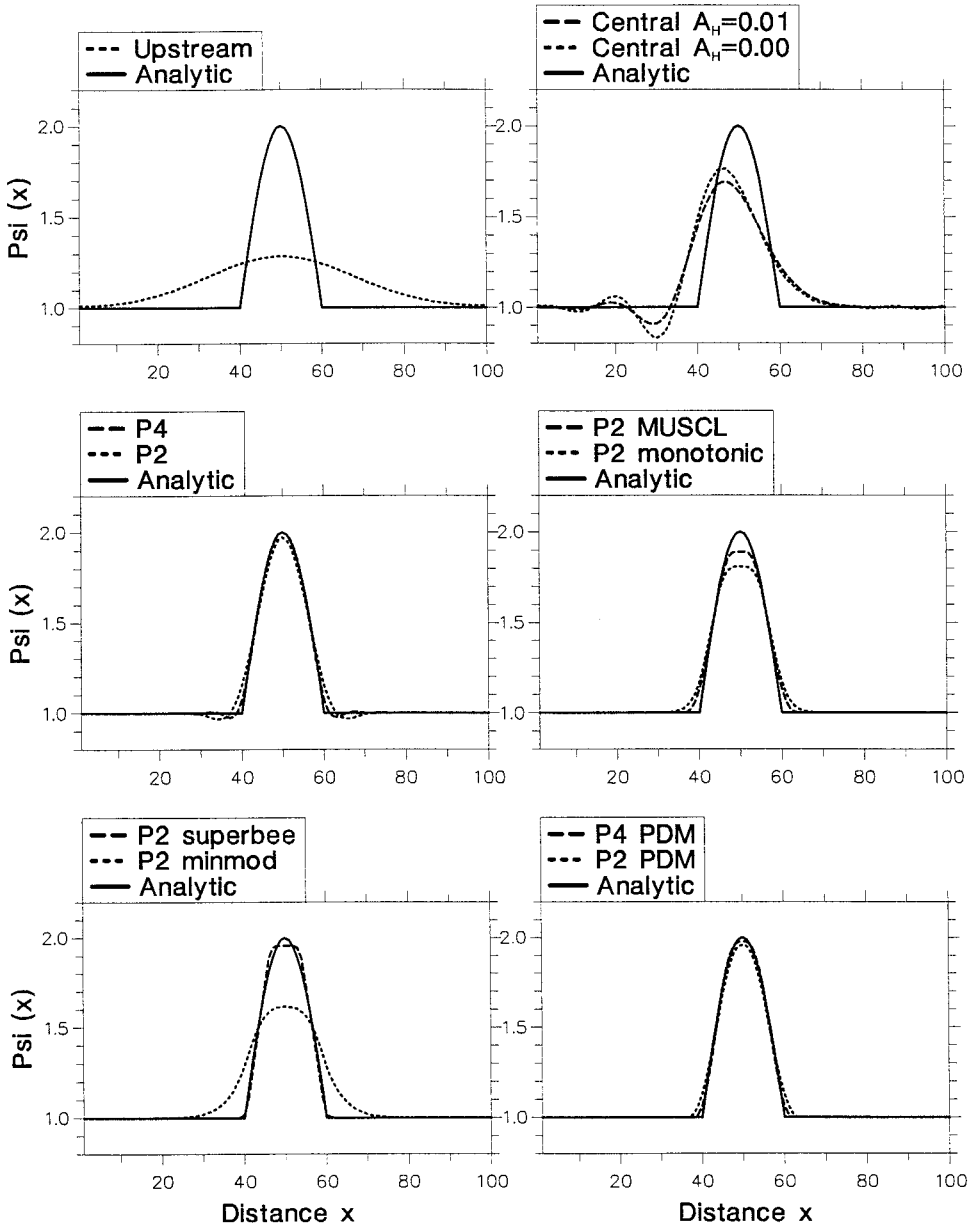

FIG. 2. A comparison of the advection schemes with the analytic solution showing the initial semicircle and the numerical solution after six rotations through the domain.

with a constant angular velocity of $\omega = 0.1\ s^{-1}$ and a rotation center located at $(x_0, y_0) = (50\Delta x, 50\Delta y)$. A time step of $\Delta t = 0.1$ is used so that 628 time steps is equivalent to one full rotation. The maximum Courant number in the domain is 0.7 and three classic initial conditions are used, a cube, a cone, and a slotted cylinder, superimposed on a background field of 1.0. The cube has a height of 4.0 with lateral lengths of $20\Delta x$ centered at $x = 30\Delta x$; $y = 70\Delta y$. The cone has a base radius of $15\Delta x$ and a maximum height of 4.0 at $(x_m, y_m) = (50\Delta x, 75\Delta y)$. The slotted cylinder has a height of 4.0 centered at $x = 70\Delta x$, $y = 50\Delta y$ with base radius $15\Delta x$ containing a groove of $6\Delta x$ and length of $20\Delta x$. At the open boundaries, the first spatial partial derivative in the normal direction was assumed to vanish at an outflow boundary, while the undisturbed initial value of the field was assumed at an inflow boundary.

The one-dimensional tests demonstrated the superior performance of the PDM limiter [see Pietrzak (1995) for other examples]. Only the PDM limiter is included in the two-dimensional examples presented here. Figure 3 shows the analytical functions used in the solid-body rotation tests. Figures 4a and 4b show the P2 and P2_PDM scheme after six revolutions through the do-

TABLE 1a. Conservation squared (Err2); L_2 error; absolute maximum and minimum values during the run, maximum and minimum values after six rotations; and CPU time relative to the upstream scheme for advection of the square with a Courant number of 0.5.

Scheme	Err2	L_2 error	Abs. min.	Abs. max.	Final min.	Final max.	CPU
P0 (upstream)	0.91	0.31	1.00	2.00	1.02	1.42	1.0
Central $A_H = 0$	0.97	0.17	0.61	2.38	0.89	2.06	1.2
Central $A_H = 0.01$	0.96	0.18	0.64	2.37	0.92	1.93	1.3
P2	0.99	0.12	0.93	2.08	0.95	2.08	2.1
P2_minmod	0.96	0.16	1.00	2.00	1.00	1.83	2.2
P2_monotonic	0.96	0.12	1.00	2.00	1.00	1.97	2.3
P2_MUSCL	0.98	0.12	1.00	2.00	1.00	2.00	2.3
P2_Superbee	0.99	0.07	1.00	2.00	1.00	2.00	2.3
P2_PDM	0.98	0.12	1.00	2.00	1.00	2.00	2.5
P4	0.99	0.09	0.91	2.09	0.93	2.07	2.5
P4_PDM	0.99	0.09	1.00	2.00	1.00	2.00	2.9

TABLE 1b. As in Table 1a but for the advection of the semicircle.

Scheme	Err2	L_2 error	Abs. min.	Abs. max.	Final min.	Final max.	CPU
P0 (upstream)	0.95	0.24	1.00	2.00	1.01	1.28	1.0
Central $A_H = 0$	0.98	0.14	0.83	2.03	0.83	1.76	1.2
Central $A_H = 0.01$	0.98	0.14	0.91	2.01	0.91	1.69	1.3
P2	1.00	0.03	0.97	2.00	0.97	1.97	2.1
P2_minmod	0.97	0.12	1.00	2.00	1.00	1.62	2.2
P2_monotonic	0.97	0.05	1.00	2.00	1.00	1.81	2.3
P2_MUSCL	0.99	0.03	1.00	2.00	1.00	1.89	2.3
P2_Superbee	1.00	0.02	1.00	2.00	1.00	1.96	2.3
P2_PDM	0.99	0.03	1.00	2.00	1.00	1.95	2.5
P4	1.00	0.01	0.98	2.00	0.98	2.00	2.5
P4_PDM	1.00	0.01	1.00	2.00	1.00	1.98	2.9

main, while Figs. 5a and 5b illustrate the corresponding results for the P4 and P4_PDM schemes. The unlimited constant grid flux form schemes P2 and P4 are prone to numerical dispersion. This is clearly highlighted by the dispersive ripples at the base of the functions and the overshooting at their tops. In contrast the PDM limited schemes are monotone, have better amplitude and shape preserving properties, and are almost as computationally efficient as the unlimited schemes. The unlimited schemes exhibit better amplitude preservation as expected since the limiters introduce some numerical diffusion. These results are also confirmed in Tables 2a–c. The upstream and central leapfrog scheme are also given. The under- and overshooting of the leapfrog scheme and the numerical diffusion of the upstream scheme is evident. Again, the P2 and P2_PDM schemes are only twice as expensive as the leapfrog scheme.

c. *Deformational flow fields*

In order to assess the time-splitting error, the deformational flow field test (Smolarkiewicz 1982), for which Staniforth et al. (1987) provided the analytical solution for short time integrations, is carried out. The streamfunction distribution employed yields a strongly deformational flow field consisting of sets of symmetrical vortices. Each vortex occupies a square with lateral lengths of 25 grid points. Fluid elements are constrained to move along streamlines and cannot escape from the vortex in which they are located at the initial time. Since the initial tracer concentration occupies six vortices it should be distributed over these six vortices for all time. The cone distribution described above is superimposed on a background concentration tracer field of 1.0 and a time increment of $\Delta t = 0.7$ s is used.

Figures 6a, 6b, and 6c show the results with and without the second-order velocity corrections discussed in section 2 and with the Easter method combined with Strang splitting, after 19, 38, 57, and 76 time steps. Only

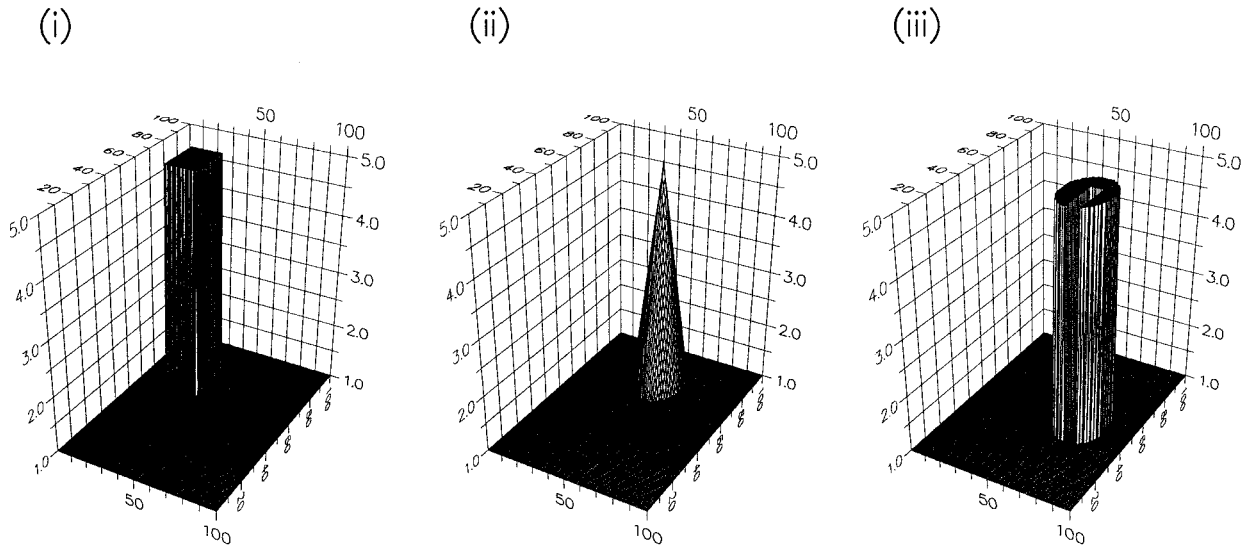

FIG. 3. Initial distribution and analytic solution for the cube, cone, and slotted cylinder after six revolutions through the domain.

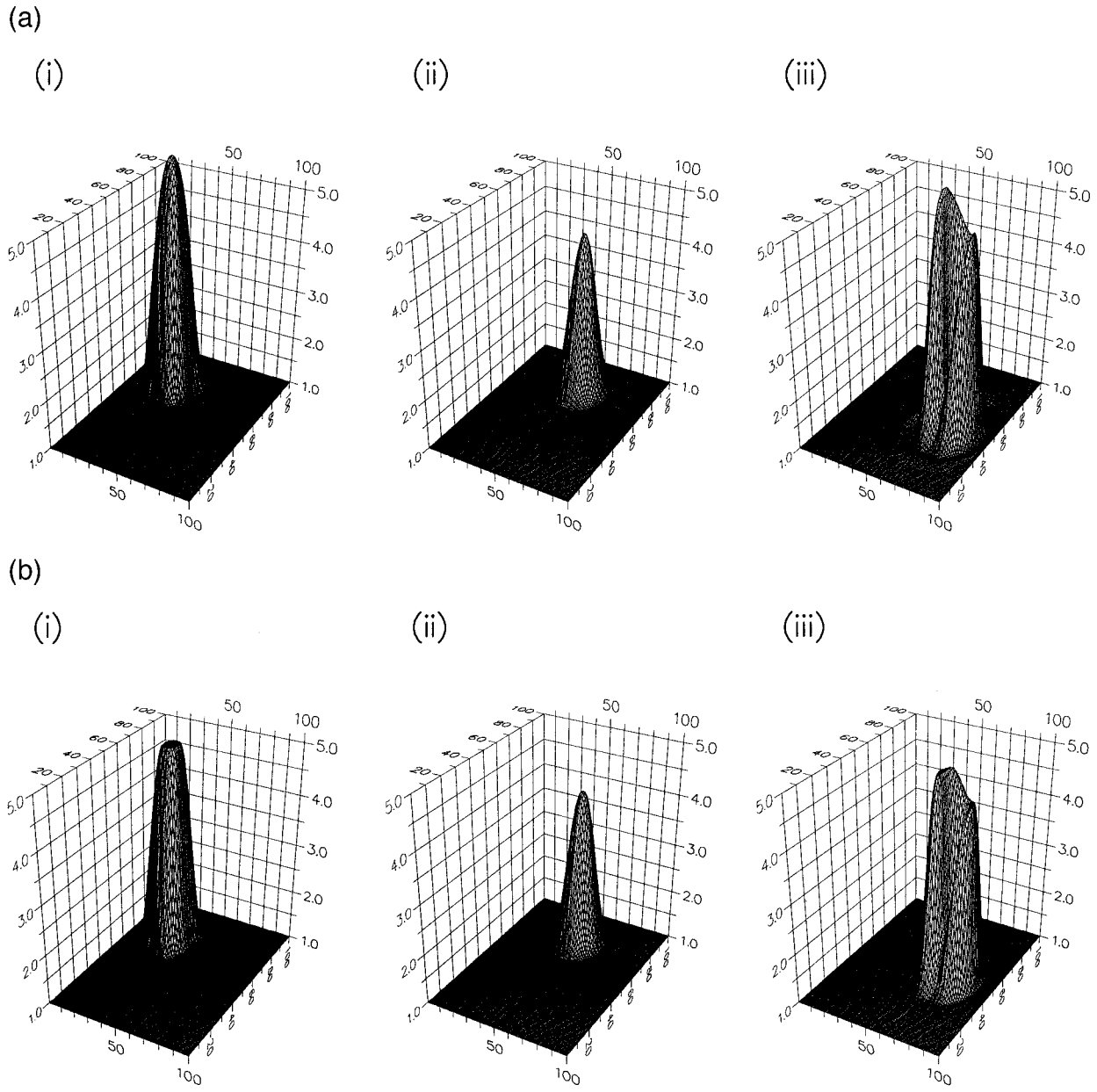

FIG. 4. Numerical solutions for the rotating cube, cone, and slotted cylinder using the (a) P2 and (b) P2_PDM schemes after six revolutions through the domain.

the P2_PDM scheme is shown, in order to highlight the potential time-splitting errors in a variable flow field. The first-order time-splitting error is evident in Fig. 6a. The simple second-order-accurate corrections significantly reduce this error. Strang splitting also reduces this error, giving results slightly better than those in Fig 6b, but at an increase in computational cost. The method of Easter combined with Strang splitting, Fig 6c, gives the best results, preserving a constant mixing ratio. However, all the constant grid flux form schemes (not shown) exhibited reasonable agreement with the analytical solution given by Staniforth et al. (1987). In addition, further tests using a zero background tracer field, demonstrated that both the P2_PDM and P4_PDM are positive definite. An advantage of the limited schemes is that despite the fact that they are not strictly TVD in a two-dimensional flow field they exhibit nearly monotone behavior. This is true in a deformational flow field if the time-splitting errors are corrected.

d. Three-dimensional primitive equation experiments

In order to test the suitability of the forward-in-time upstream-weighted schemes, P2_PDM, and P4_PDM,

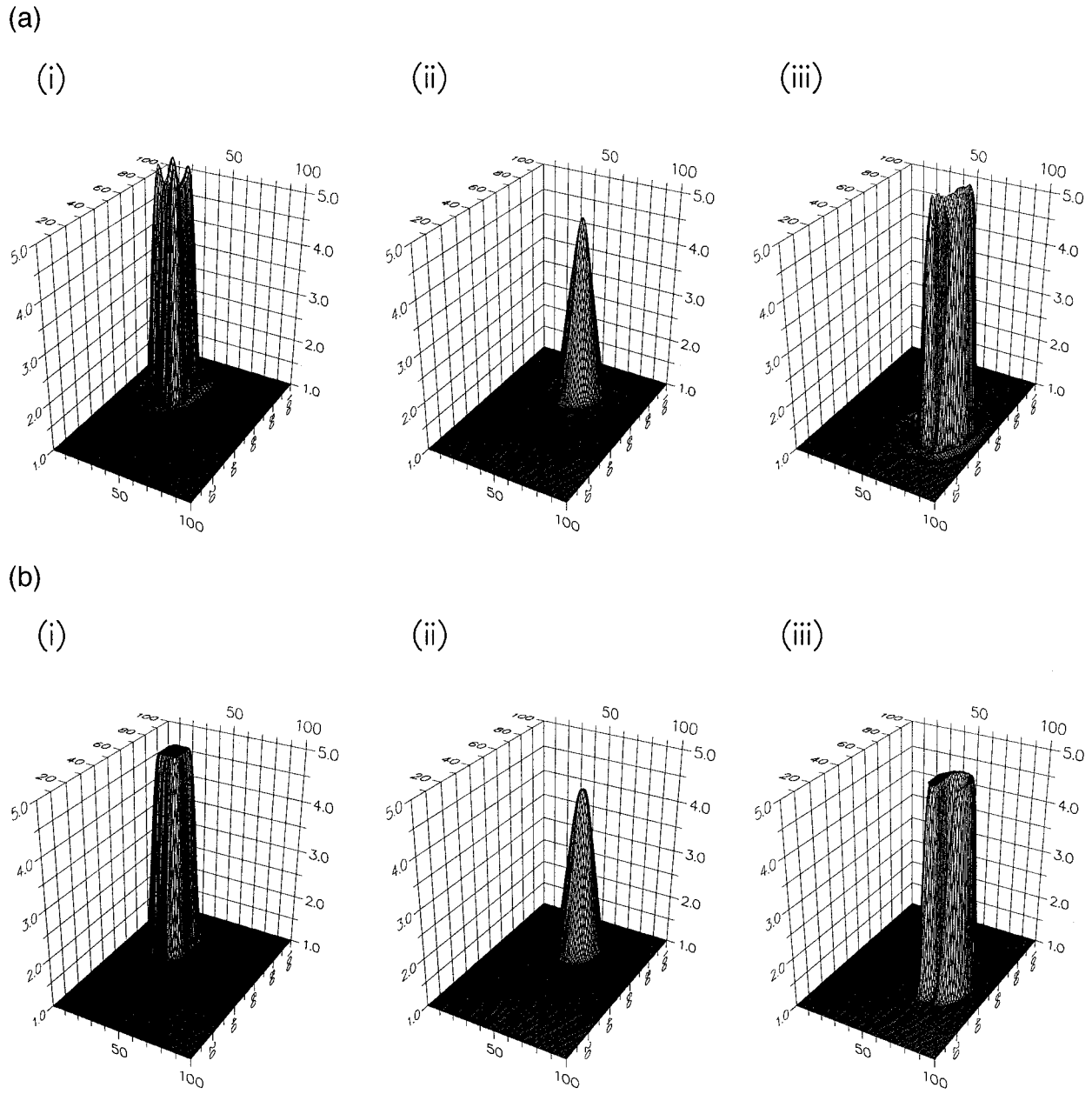

FIG. 5. Numerical solutions for the rotating cube, cone, and slotted cylinder using the (a) P4 and (b) P4_PDM schemes after six revolutions through the domain.

for coastal ocean modeling, a number of three-dimensional primitive equation test cases were carried out. They included an idealized lock exchange test and a coastal simulation in the Danish Sound. The CGF schemes were applied to temperature and salinity, not momentum. Their performance was also compared against the central difference scheme as this is used in the original POM. In both examples, a grid size of 1 km was chosen, with an internal baroclinic time step of 100 s, an external barotropic time step of 10 s, and 11 sigma levels in the vertical. The different time steps arise because the POM uses a mode-splitting technique that allows a separation between the frequency of calculation of the barotropic and baroclinic time steps.

Figure 7 shows a vertical salinity section taken along the center of the numerical tank used in the lock-exchange tests after 5 h. In the experiment the fluid on the right-hand side initially has a salinity of 30 psu and temperature of 10°C and is separated, by an imaginary barrier, from the fluid on the left-hand side, which has a salinity of 25 psu and temperature of 5°C. This is equivalent to a density difference of 3.5 kg m^{-3}. As

TABLE 2a. Conservation squared (Err2); L_2 error; absolute maximum and minimum values during the run; maximum and minimum values after six rotations; and CPU time relative to the upstream scheme for advection of the cube, superimposed on a background tracer value of 1.0, for $c = 0.5$.

Scheme	Err2	L_2 error	Abs. min.	Abs. max.	Final min.	Final max.	CPU
Upstream	0.59	0.78	1.00	5.00	1.00	1.44	1.0
Central $A_H = 0$	0.91	0.50	−1.34	8.16	−0.03	5.90	1.3
Central $A_H = 0.01$	0.87	0.48	−1.05	8.05	0.39	5.38	1.3
P2	0.93	0.33	0.43	5.85	0.75	5.63	2.6
P4	0.97	0.24	0.29	6.08	0.63	5.60	3.5
P2_PDM	0.90	0.32	1.00	5.00	1.00	5.00	2.6
P4_PDM	0.94	0.25	1.00	5.00	1.00	5.00	4.0

soon as the experiment starts, the dense fluid starts to collapse and countercurrents begin to flow in opposite directions. These consist of a gravity current of less dense fluid moving along the surface and a dense current flowing beneath it in the opposite direction. The flow is slightly asymmetrical, with retardation occurring near the bed, due to the bottom friction. The propagation speed of the density front can be determined by equating the decrease of potential energy with the increase of kinetic energy and is given by $U_0 = 0.5(g'H)^{1/2}$, where g' is the reduced gravity and H is the full depth of the fluid. This value is known to be in reasonable agreement with experimental values obtained in enclosed wide conduits of about $0.44(g'H)^{1/2}$. Experimental results from channels with a free surface show that the flow becomes asymmetrical with corresponding multiplying constants of 0.47 for the underflow and 0.59 for the overflow (Simpson 1987). Inserting these experimental values suggests propagation speeds of 0.36 m s^{-1} for the lower layer and 0.49 m s^{-1} for the upper layer. While all the simulated propagation speeds are in reasonable agreement with these values, a significant difference is observed in the evolution of the stratification. The central scheme exhibits significant over- and undershoot, with salinity minima and maxima exceeding 23 and 32 psu, respectively. The usual technique to suppress this type of rippling is to use higher values of the Smagorinsky coefficient in the horizontal formulation of the diffusivity. The value used here was 0.1 and typical values range from 0.05 to 0.3. However, larger values lead to greater damping of the solution and smearing of the interface. More importantly it highlights the subjective choice of the coefficients, which have more to do with numerical stability than physical reasoning. In contrast the higher-order schemes give much better results, with much smaller under- and overshoot, typically less than 0.1 psu. The results only improve slightly with the order of the scheme and they are similar for all the constant grid flux form schemes. The P4 solution (not shown) is similar to the P2 example and both schemes are dispersive. The limiters (Fig. 7) eliminate the overshooting that is observed in the time evolution of the front. The

TABLE 2b. As in Table 2a but for the advection of the cone.

Scheme	Err2	L_2 error	Abs. min.	Abs. max.	Final min.	Final max.	CPU
Upstream	0.82	0.39	1.00	5.00	1.00	1.27	1.0
Central $A_H = 0$	0.98	0.21	0.58	5.00	0.58	3.90	1.3
Central $A_H = 0.01$	0.97	0.20	0.70	5.00	0.70	3.59	1.3
P2	0.99	0.04	0.95	5.00	0.95	4.25	2.0
P4	1.00	0.03	0.96	5.00	0.96	4.60	3.4
P2_PDM	0.98	0.04	1.00	5.00	1.00	4.16	2.6
P4_PDM	1.00	0.03	1.00	5.00	1.00	4.32	4.0

PDM limiter gives a positive definite and effectively nonoscillatory solution. The PDM limiter introduces a minimal amount of implicit diffusion and does not distort the shape of the interface, having nearly identical results to the unlimited versions. The Superbee limiter steepens the front, in comparison with the unlimited scheme, while the minmod limiter is more diffusive. In these tests the PDM limiter remains positive definite for Courant numbers less than one, in contrast to the other limiters which are positive definite for Courant numbers less than 0.5 (Pietrzak 1995). However, all the limiters show a significant improvement over the central scheme. The PDM limiter was found to be the best overall choice of the limiters, giving high resolution of the interface with minimal implicit diffusion and exhibiting an effectively nonoscillatory behavior.

The Øresund Sound is one of three channels that forms part of the transition region connecting the fresher waters of the Baltic Sea with the saltier North Sea (Fig. 8). It is a region of complex bathymetry, with a narrow channel in the north separating Denmark and Sweden and the Drogden Sill to the south. It is subject to large salinity gradients, typically 8 psu in the south and 23 psu in the north. The Drogden Sill is one of the two sills that controls the inflow of saline water to the Baltic. In this sense it is an ideal region with which to compare the schemes, being a tough test of their positive definite and monotone claims, particularly in light of the results of section 3c. Therefore a lock exchange–type test was set up in the sound with a domain of 121 km in the north–south direction and 61 km in the east–west direction. The more saline and colder water in the north (23 psu and 11°C) was separated from the less saline and warmer water in the south (8 psu and 16°C) by an

TABLE 2c. As in Table 2a but for the advection of the slotted cylinder.

Scheme	Err2	L_2 error	Abs. min.	Abs. max.	Final min.	Final max.	CPU
Upstream	0.58	0.83	1.00	5.00	1.00	1.85	1.0
Central $A_H = 0$	0.93	0.73	−2.22	7.58	−1.54	5.71	1.3
Central $A_H = 0.01$	0.85	0.64	−1.97	7.43	−0.21	5.05	1.3
P2	0.89	0.39	0.11	5.78	0.78	5.53	2.0
P4	0.96	0.29	−0.14	6.02	0.24	5.64	3.5
P2_PDM	0.87	0.40	1.00	5.00	1.00	5.00	2.6
P4_PDM	0.94	0.25	1.00	5.00	1.00	5.00	4.0

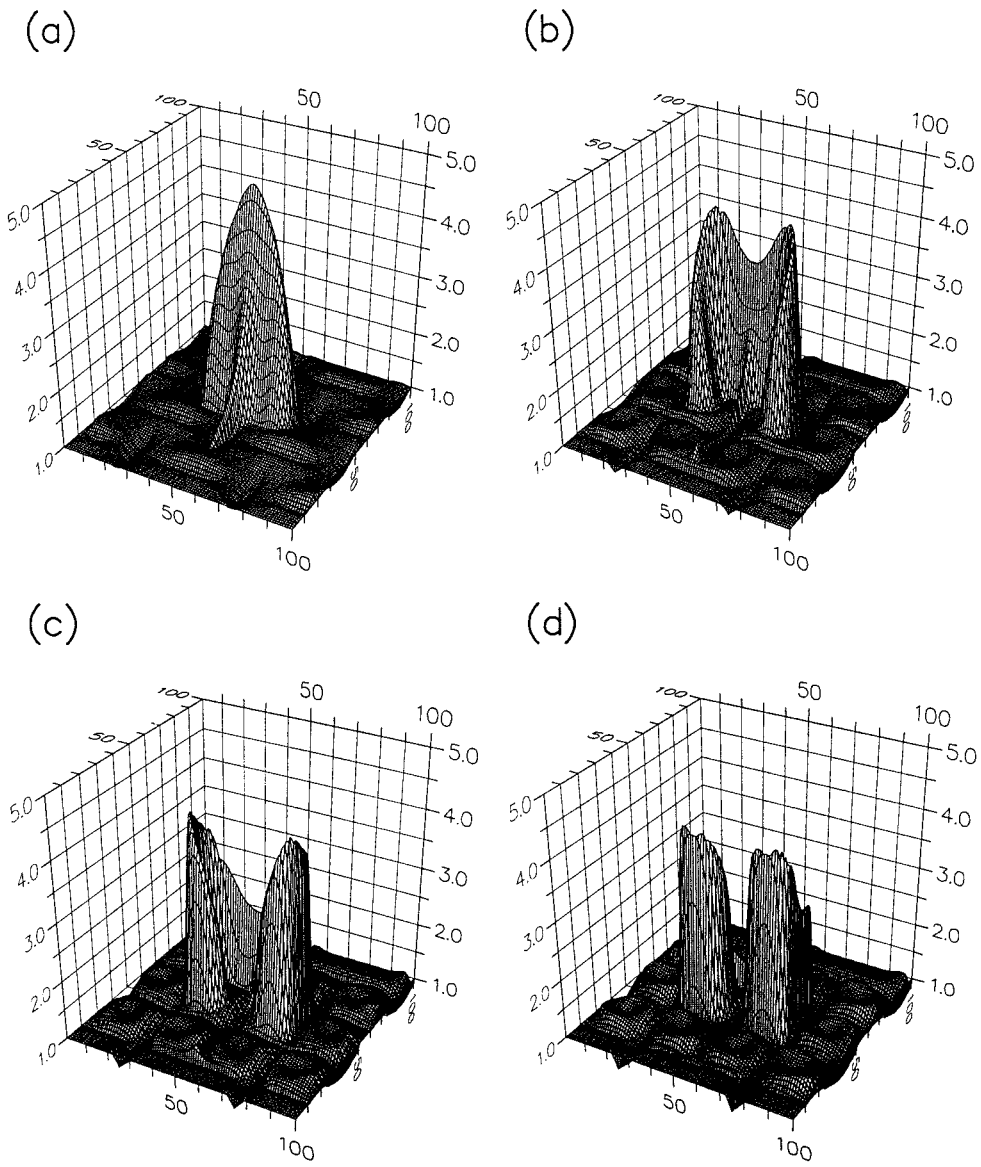

FIG. 6a. Deformational flow test showing the numerical solution using the original P2_PDM scheme after (a) 19 time steps, (b) 38 time steps, (c) 57 time steps, and (d) 76 time steps.

imaginary barrier at the midpoint of the north–south domain. Figure 8a shows the surface salinity after 4 days, highlighting the sharp salinity front that develops in the surface and the strongly converging flow in the northern bottleneck.

The central-difference scheme leads to greater over- and undershoot in the numerical solutions with extreme values less than 5 psu and in excess of 25 psu. The unlimited P2 and P4 schemes also exhibit some over- and undershoot of the order 1.0 psu, but it is much less than found in the central scheme. The P2_PDM and P4_PDM schemes combined with Strang splitting give an effectively nonoscillatory performance, are positive definite, and have an extreme overshoot of only 0.01 psu (at an increase in computational cost). If the modified velocity field method is used, the scheme remains positive definite but now has an overshoot of 0.1 psu. The degradation in performance compared with the results of section 3c suggest that the land boundaries might reduce the second-order velocity corrections to first order in their vicinity. However, it is worth noting that if neither Strang splitting nor the modified velocity field method are used, the scheme remains positive definite, only exhibiting mild overshooting of the order 0.5 psu. This cheaper computational alternative might be the best compromise in many practical cases. The sound example presented here is an extreme test of the schemes, in particular, as the surface front flows into the con-

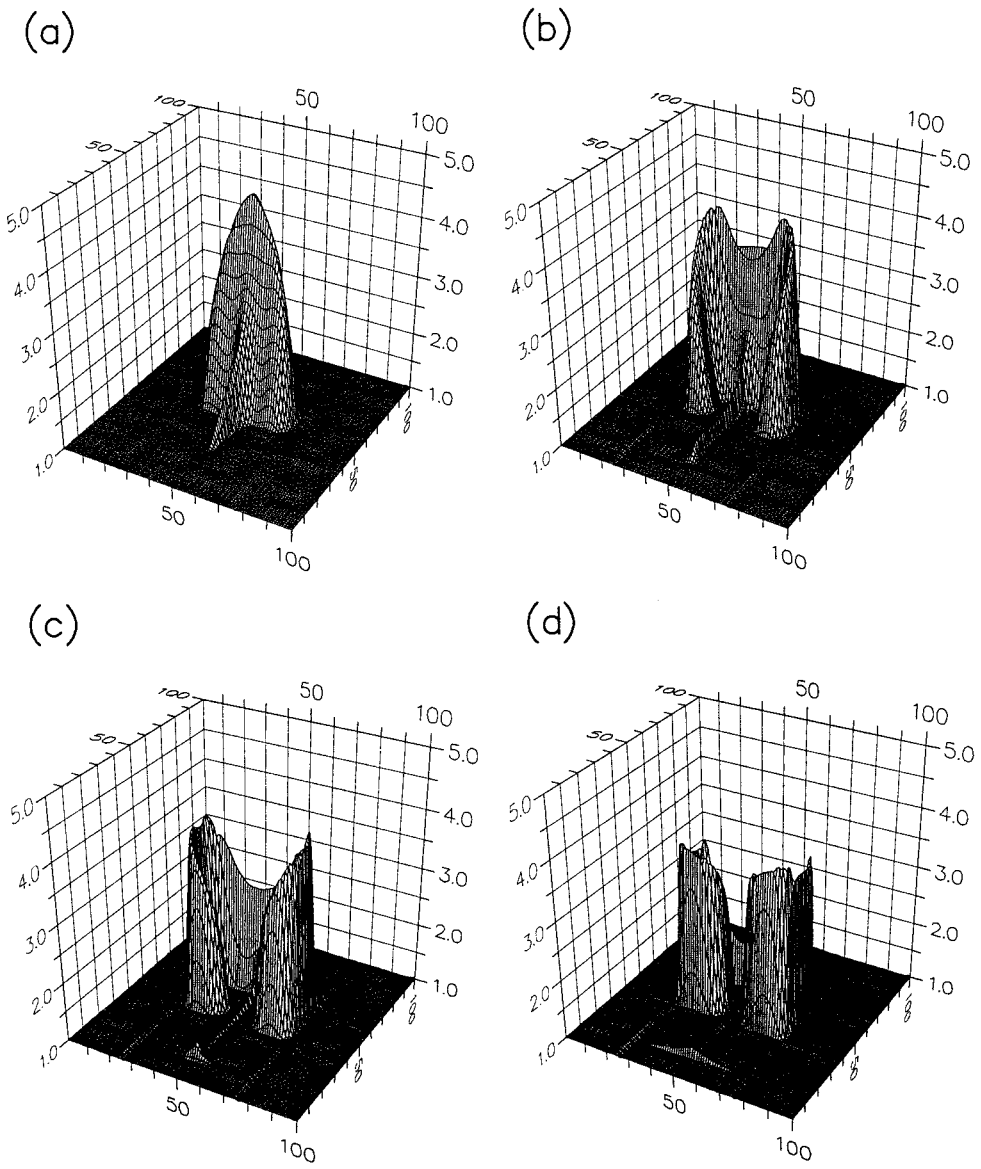

FIG. 6b. Deformational flow test showing the numerical solution using the P2_PDM scheme, with the modified velocity field corrections, after (a) 19 time steps, (b) 38 time steps, (c) 57 time steps, and (d) 76 time steps.

verging northern region, it flows along the diagonal. Consequently the cross-derivative terms become important. In many simulations this is not the case and cheaper computational results are possible. The P4 and P4_PDM schemes do not show a marked improvement over the P2 and P2_PDM schemes. The effects of the complex land boundaries are again felt, with the land boundaries reducing the order of the polynomial fitting in their vicinity and thereby reducing the overall accuracy. Of the higher-order schemes the P2_PDM scheme seems to be the best compromise between increased accuracy and computational efficiency. In the examples presented here the P2 scheme typically requires 35% more time than the central scheme, the P4 scheme requires 52% more time, and the PDM limiter adds another 5%. These results are sensitive to the baroclinic/barotropic mode-splitting ratio employed. In the current tests this is only a factor of 10, therefore 10 barotropic time steps are taken for every baroclinic time step. In many coastal simulations this is much bigger, in which case the computational cost of the higher-order schemes would be lower.

It is worth noting that limited schemes are strictly TVD only in the one-dimensional case (Goodman and LeVeque 1985). However, as discussed by LeVeque (1992) numerical methods obtained using high-resolution one-dimensional methods combined with Strang splitting typically work well in practice. They remain

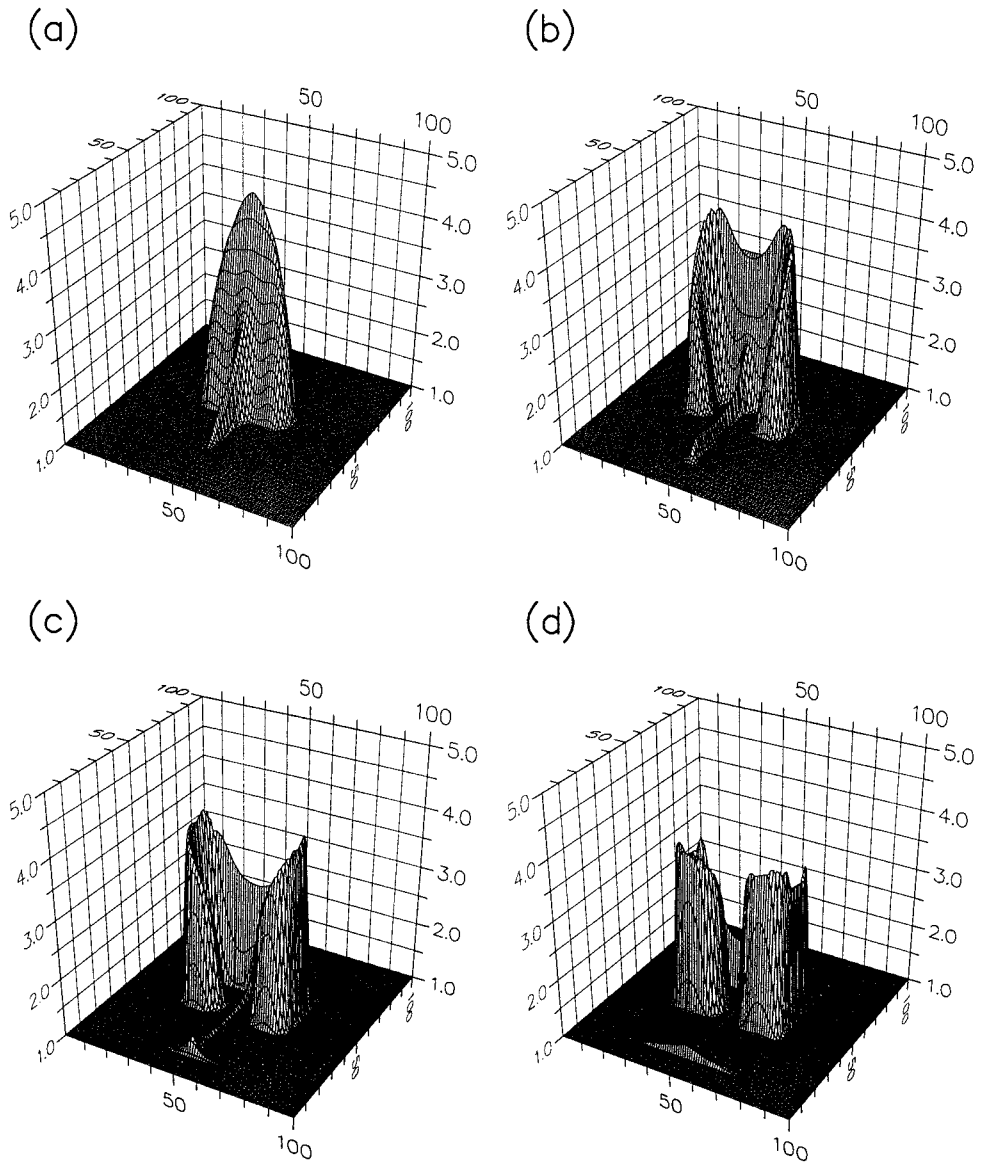

FIG. 6c. Deformational flow test showing the numerical solution using the P2_PDM scheme, with the method of Easter and Strang splitting, after (a) 19 time steps, (b) 38 time steps, (c) 57 time steps, and (d) 76 time steps.

second-order accurate on smooth solutions and usually give nonoscillatory solutions near discontinuities, as clearly shown by the Sound experiments. If a fully second-order-accurate scheme is necessary, then either a predictor–corrector method combined with Strang splitting could be developed or the modified velocity method, including the temporal modifications, can be used. Either method in combination with the method described by Easter (1993) works well in the examples given here. The most accurate method is found in combination with Strang splitting. This is because averaging is required with the modified velocity method which leads to a loss of accuracy, particularly near the land boundaries.

4. Discussion

This paper explored the suitability of nonoscillatory forward-in-time upstream-weighted differencing to the advection of scalars in three-dimensional primitive equation modeling. It was motivated by the need to investigate alternative schemes for the advection of fields with large gradients in numerical ocean modeling. The leapfrog central-difference scheme, which is still in widespread use in a number of ocean models, was compared with alternative schemes that combined the constant grid flux form philosophy of Tremback et al. (1987) with TVD flux limiters and the modified time-splitting approach of Easter (1993). The latter method

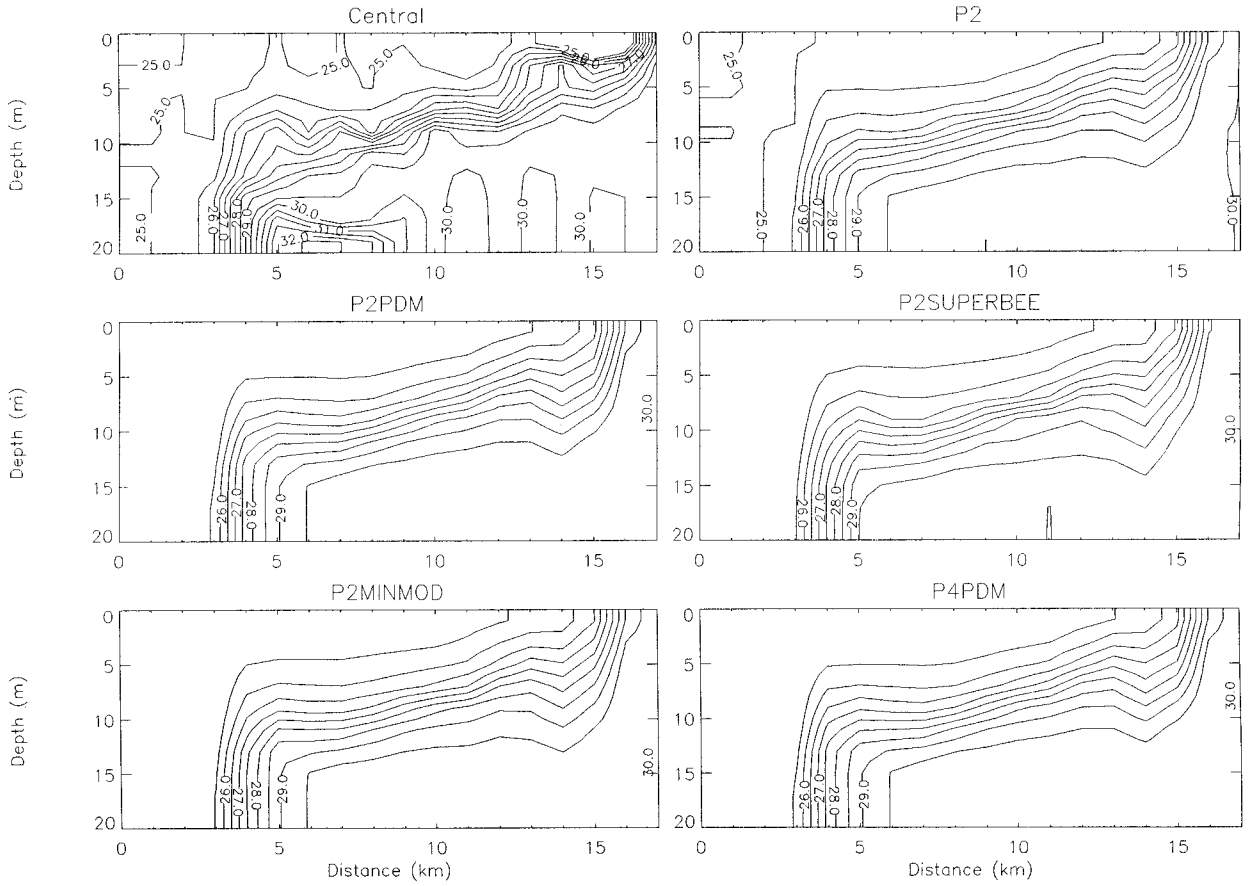

FIG. 7. A comparison of the effect of the different advection schemes on the solution of the lock exchange experiment.

was found to be necessary if time splitting was used in the development of fully three-dimensional schemes.

A comprehensive series of numerical experiments were described. The classic one- and two-dimensional test cases showed that the limited schemes compare well with other schemes in the literature. For example, Lin et al. (1994) used the van Leer scheme while James (1996) compared both the third-order PPM scheme and the second-order Lax–Wendroff scheme (similar to a P1 scheme) with the Superbee limiter. The higher-order PPM scheme is much less diffusive than the van Leer scheme and also gave much better resolution of fronts than the Lax–Wendroff scheme. However, it has a significant computational overhead. The extensive tests presented here highlighted that higher-order TVD limited schemes can easily be developed as in the two presented here, the P2_PDM and P4_PDM. The PDM limiter was selected because detailed one-dimensional tests demonstrated its superior performance over a number of other limiters commonly referenced in the literature. These schemes are nonoscillatory for Courant numbers less than one and are found to be suitable for primitive equation modeling. They are easy to implement and computationally efficient, giving well-resolved discontinuities.

All the numerical tests, including the more realistic lock-exchange and coastal front simulations, demonstrated the dispersive nature of the leapfrog scheme. The numerical dispersion severely corrupted the flow with under- and overshooting values. In addition, the method of introducing a small amount of diffusion to control this problem is highly subjective. The results presented here suggest that higher-order nonoscillatory forward-in-time advection schemes are suitable alternatives for ocean modeling. Although consideration has been given to flows in frontal regions, the problem is more widespread than just coastal ocean modeling. For example, Hecht et al. (1995) recently compared a number of schemes suitable for the advection of tracers in two-dimensional ocean models. They also demonstrated the importance of higher-order forward-in-time schemes in large-scale ocean modeling.

On a more cautionary note, further research is required before the real benefits of these types of schemes for general three-dimensional primitive equation modeling are known. The idealized tests demonstrated an improved performance of the P4 schemes over the P2 schemes. This is in accordance with the results of Tremback et al. (1987), who found an improved performance for polynomials up to 6. In more practical ocean ap-

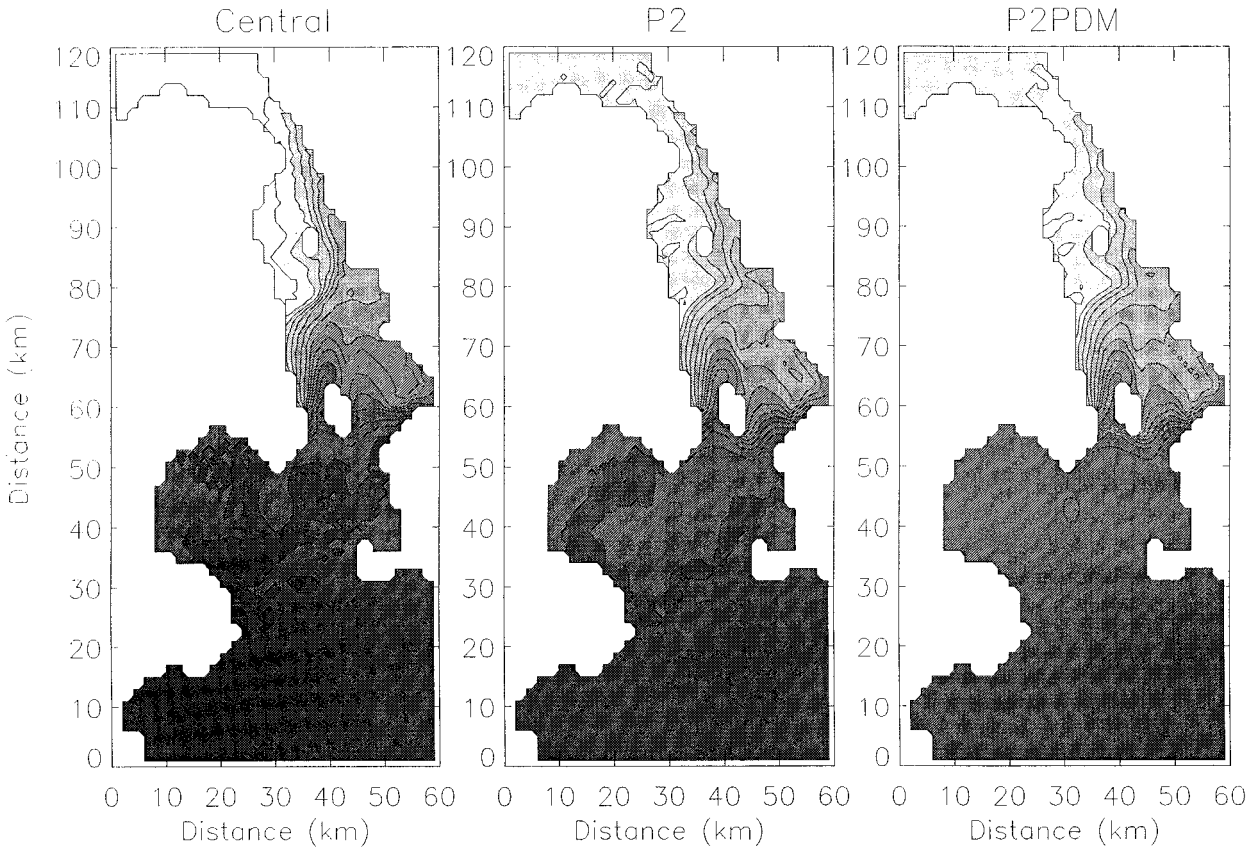

FIG. 8. A comparison of the influence of the Central, P2 and P2_PDM advection schemes on the solution of the surface salinity field after 4 days.

plications, however, land boundaries need to be taken into account. They impose a restriction on the size of the stencil used in the advection scheme and thereby limit the overall order of accuracy achieved because low-order polynomials are used at the land boundaries.

Ongoing research currently involves the application of these methods to more realistic simulations. Many questions remain about the advantages and disadvantages of these schemes. For example, they work by effectively combining the constant grid flux form method, which by construction is always used in smooth regions, with the total variation diminishing flux limiters, which are only used in regions with steep gradients. The PDM limiter has the advantage of introducing minimal diffusion while resolving discontinuities. However, the influence of this implicit numerical diffusion needs to be carefully addressed, in particular, where these types of schemes are used in studies of the physics of coastal flows. Finally, the recent work of Roache (1992), Hundsdorfer and Spee (1995), and Lin and Rood (1996) shows that the CGF methodology can be adapted so that the CFL restriction can be removed. The application of these concepts in ocean modeling is therefore an important area of future research.

Acknowledgments. The author wishes to thank Erik Berge and Eivind Martinsen for originally suggesting the use of the constant grid flux form schemes and George Mellor and Alan Blumberg for making their ocean model available. Most of this work was carried out while at the Danish Meteorological Institute and I would like to thank my colleagues Jacob Woge Nielsen, Karsten Bolding, and Nicolai Kliem for their help and many discussions. I would also like to thank two anonymous reviewers, one of whom substantially improved the manuscript, and I would like to thank John Thuburn for making a preprint of his note on TVD schemes available. Finally I would like to thank the Danish National Research Foundation for financial support.

APPENDIX

Strang Splitting and the Modified Velocity Method

Following Hundsdorfer and Trompert (1994) Eq. (1) can be rewritten as

$$\frac{\partial \hat{\psi}}{\partial t} + A\hat{\psi} + B\hat{\psi} + C\hat{\psi} = 0, \qquad \text{(A1)}$$

where

$$A\hat{\psi} = \frac{\partial u\hat{\psi}}{\partial x}, \qquad B\hat{\psi} = \frac{\partial v\hat{\psi}}{\partial y}, \qquad C\hat{\psi} = \frac{\partial \omega\hat{\psi}}{\partial \sigma}. \quad \text{(A2)}$$

It should be noted that substituting $\hat{\psi} = \psi$ and z for σ gives the z coordinate system used in Eq. (1), whereas $\hat{\psi} = \psi D$ gives Eq. (20), and $\hat{\psi} = D$ gives Eq. (21) in the σ coordinate system used in the POM.

The exact solution of Eq. (A1) satisfies

$$\hat{\psi}(t_{n+1}, x, y, \sigma) = e^{-\Delta t(A+B+C)}\hat{\psi}(t_n, x, y, \sigma), \quad \text{(A3)}$$

where the exponential of the solution operator is defined by the power series of the exponential function. Time splitting solves a series of 1D problems, giving instead

$$\hat{\psi}(t_{n+1}, x, y, \sigma) = e^{-\Delta tC}e^{-\Delta tB}e^{-\Delta tA}\hat{\psi}(t_n, x, y, \sigma). \quad \text{(A4)}$$

A second-order-accurate solution is therefore equivalent to the time-split version plus the truncation error terms, that is

$$\begin{aligned} e^{-\Delta t(A+B+C)}\hat{\psi}(t_n, x, y, \sigma) &= e^{-\Delta tC}e^{-\Delta tB}e^{-\Delta tA}\hat{\psi}(t_n, x, y, \sigma) + \frac{1}{2}\Delta t^2\hat{\psi} \\ &\times [(AB - BA) + (AC - CA) + (BC - CB)] \\ &+ O(\Delta t^3), \end{aligned} \quad \text{(A5)}$$

where

$$(AB - BA)\hat{\psi} = -\frac{\partial}{\partial x}\left(\frac{\partial u}{\partial y}v\hat{\psi}\right) + \frac{\partial}{\partial y}\left(u\frac{\partial v}{\partial x}\hat{\psi}\right) \quad \text{(A6)}$$

$$(AC - CA)\hat{\psi} = -\frac{\partial}{\partial x}\left(\frac{\partial u}{\partial \sigma}\omega\hat{\psi}\right) + \frac{\partial}{\partial \sigma}\left(u\frac{\partial \omega}{\partial x}\hat{\psi}\right) \quad \text{(A7)}$$

$$(BC - CB)\hat{\psi} = -\frac{\partial}{\partial y}\left(\frac{\partial v}{\partial \sigma}\omega\hat{\psi}\right) + \frac{\partial}{\partial \sigma}\left(v\frac{\partial \omega}{\partial y}\hat{\psi}\right). \quad \text{(A8)}$$

This illustrates the introduction of the first-order error by the time-splitting procedure. A second-order accurate scheme can be maintained however, with Strang splitting (LeVeque 1992). Using this technique, the one-dimensional subprocesses are interchanged after each time step:

$$\hat{\psi}^{n+1}(x, y, \sigma) = e^{1/2(\Delta tA)}e^{1/2(\Delta tB)}e^{\Delta tC}e^{1/2(\Delta tB)}e^{1/2(\Delta tA)}\hat{\psi}^n \times (x, y, \sigma). \quad \text{(A9)}$$

However, unlike the two-dimensional case, which involves a sequence of alternating steps $\frac{1}{2}x - y, y - x, x - \frac{1}{2}y$, this technique involves a more substantial increase in computational time.

Instead Hundsdorfer and Trompert (1994) suggested simply modifying the velocity field in order to achieve a second-order scheme and this approach is adopted in the following section for the three-dimensional case. A second-order-accurate upstream advection scheme can be achieved by modifying the velocity field so that the first-order error terms arising from both the splitting error and the assumption of a constant flow field are compensated. Equation (1) can be approximated as

$$\frac{\partial \hat{\psi}}{\partial t} + \frac{\partial \tilde{u}\hat{\psi}}{\partial x} + \frac{\partial \tilde{v}\hat{\psi}}{\partial y} + \frac{\partial \tilde{\omega}\hat{\psi}}{\partial \sigma} = 0 \quad \text{(A10)}$$

with the modified velocity field given by

$$\tilde{u} = u - \frac{1}{2}\Delta t\left(u\frac{\partial u}{\partial x} - v\frac{\partial u}{\partial y} - \omega\frac{\partial u}{\partial \sigma}\right) \quad \text{(A11)}$$

$$\tilde{v} = v - \frac{1}{2}\Delta t\left(v\frac{\partial v}{\partial y} + u\frac{\partial v}{\partial x} - \omega\frac{\partial v}{\partial \sigma}\right) \quad \text{(A12)}$$

$$\tilde{\omega} = \omega - \frac{1}{2}\Delta t\left(\omega\frac{\partial \omega}{\partial \sigma} + u\frac{\partial \omega}{\partial x} + v\frac{\partial \omega}{\partial y}\right), \quad \text{(A13)}$$

which is accurate to second order in space. Care must be taken to maintain a conservative discretization of the modified velocity field. In sigma coordinates it is important to use the modified velocity field in the mass continuity equation as well as in the advection of tracers [Eqs. (22) and (23)]. In z coordinates the modified velocity field does not necessarily satisfy a mass continuity equation.

REFERENCES

Arakawa, A., 1966: Computational design of long term numerical integration of the equations of atmospheric motion. *J. Comput. Phys.*, **1,** 119–143.

Berge, E., and J. E. Kristjansson, 1992: Numerical weather simulations with different formulations for the advection of humidity and cloud water. *Mon. Wea. Rev.*, **120,** 1584–1602.

Blumberg, A., and G. Mellor, 1987: A description of a three-dimensional coastal ocean circulation model. *Three-Dimensional Coastal Ocean Models,* N. Heaps, Ed., Coastal and Estuarine Sciences Series, 208 pp.

Boris, J. P., and D. L. Book, 1976: Flux corrected transport. I: SHASTA a fluid transport algorithm that works. *J. Comput. Phys.*, **11,** 38–69.

Bott, A., 1989a: A positive definite advection scheme obtained by nonlinear renormalization of the advective fluxes. *Mon. Wea. Rev.*, **117,** 1006–1015.

——, 1989b: Reply. *Mon. Wea. Rev.*, **117,** 2633–2636.

Carpenter, R. L., Jr., K. K. Drogemeier, P. R. Woodward, and C. E. Hane, 1990: Application of the piecewise parabolic method to meteorological modeling. *Mon. Wea. Rev.*, **118,** 586–612.

Collella, P., and P. R. Woodward, 1984: The piecewise parabolic method (PPM) for gas-dynamical simulations. *J. Comput. Phys.*, **54,** 174–201.

Crowley, W. P., 1968: Numerical advection experiments. *Mon. Wea. Rev.*, **96,** 1–11.

Easter, R. E., 1993: Two modified versions of Bott's positive-definite numerical advection scheme. *Mon. Wea. Rev.*, **121,** 297–304.

Goodman, J. B., and R. J. LeVeque 1985: On the accuracy of stable schemes for 2D scalar conservation laws. *Math. Comp.*, **45,** 15–21.

Harten, A., 1983: High resolution schemes for hyperbolic conservation laws. *J. Comput. Phys.*, **49,** 357–393.

——, 1984: On a class of high resolution total variation stable finite difference schemes. SIAM *J. Num. Anal.*, **21,** 1–23.

Hecht, M. W., W. R. Holland, and P. J. Rasch 1995: Upwind-weighted advection schemes for ocean tracer transport: An evaluation in a passive tracer context. *J. Geophys. Res.*, **100,** 20 763–20 778.

Hirsch, C., 1990: *Numerical Computation of Internal and External Flows.* Vol. 2, *Computational Methods for Inviscid and Viscous Flows*, John Wiley and Sons, 691 pp.

Hundsdorfer, W., and R. A. Trompert, 1994: Method of lines and direct discretisation: a comparison for linear advection. *Appl. Numer. Math.* **13,** 469–490.

——, and E. J. Spee, 1995: An efficient horizontal advection scheme for the modeling of global transport of constiuents. *Mon. Wea. Rev.,* **123,** 3554–3564.

James, I. D., 1996: Advection schemes for shelf sea models. *J. Mar. Syst.,* **8,** 237–254.

Lax, P. D., and B. Wendroff, 1964: Difference schemes with high order of accuracy for solving hyperbolic equations. *Commun. Pure Appl. Math.,* **17,** 381–398.

Leith, C. E., 1965: Numerical simulation of the earth's atmosphere. *Methods Comput. Phys.,* **4,** 1–28.

Leonard, B. P., 1979: A stable and accurate convective modelling procedure based on quadratic upstream interpolation. *Comput. Methods Appl. Mech. Eng.,* **19,** 59–98.

——, 1991: The ULTIMATE conservative difference scheme applied to unsteady one-dimensional advection. *Comput. Methods Appl. Mech. Eng.,* **88,** 17–74.

LeVeque, R. J. 1992: *Numerical Methods for Conservation Laws.* Lectures in Mathematics, Birkhauser Verlag, 214 pp.

Lilly, D. K., 1965: On the computational stability of numerical solutions of time dependent non-linear geophysical fluid dynamics problems. *Mon. Wea. Rev.,* **93,** 11–26.

Lin, S. J., and R. B. Rood, 1996: Multidimensional flux-form semi-Lagrangian transport schemes. *Mon. Wea. Rev.,* **124,** 2046–2070.

——, W. C. Chao, Y. C. Sud, and G. K. Walker, 1994: A class of van Leer–type transport schemes and its application to the moisture transport in a general circulation model. *Mon. Wea. Rev.* **122,** 1575–1593.

Mellor, G. L., and T. Yamada, 1982: Development of a turbulence closure model for geophysical fluid problems. *Rev. Geophys. Space Phys.,* **20,** 851–875.

Petschek, A. G., and L. D. Libersky, 1975: Stability, accuracy, and improvement of Crowley advection schemes. *Mon. Wea. Rev.,* **103,** 1104–1109.

Pietrzak, J. D., 1995: A comparison of advection schemes for ocean modelling. Danish Meteorological Institute Scientific Rep. 95-8, Copenhagen, Denmark, 45 pp.

Roache, P. J., 1992: A flux-based modified method of characteristics. *Int. J. Numer. Methods in Fluids,* **15,** 1259–1275.

Russell, G. L., and J. A. Lerner, 1981: A new finite-differencing scheme for the tracer transport equation. *J. Appl. Meteor.,* **20,** 1483–1498.

Simpson, J. E., 1987: *Gravity Currents. In the Environment and the Laboratory.* John Wiley and Sons. 242 pp.

Smolarkiewicz, P. K., 1982: The multidimensional Crowley advection scheme. *Mon. Wea. Rev.,* **110,** 1968–1983.

——, 1983: A simple positive definite advection transport scheme with small implicit diffusion. *Mon. Wea. Rev.,* **111,** 479–486.

——, 1984: A fully multidimensional positive definite advection transport algorithm with small implicit diffusion. *J. Comput. Phys.,* **54,** 325–362.

——, 1991: On forward-in-time differencing for fluids. *Mon. Wea. Rev.* **119,** 2505–2510.

——, and T. L. Clark, 1986: The multidimensional positive definite advection transport algorithm: Further development and applications. *J. Comput. Phys.,* **67,** 396–438.

——, and W. W. Grabowski, 1990: The multidimensional positive definite advection transport algorithm: Non oscillatory option. *J. Comput. Phys.,* **86,** 355–375.

Staniforth, A., J. Cote, and J. Pudykiewicz, 1987: Comments on ''Smolarkiewicz's deformational flow.'' *Mon. Wea. Rev.,* **115,** 540–555.

Sweby, P. K., 1984: High resolution schemes using flux limiters for hyperbolic conservation laws. *SIAM J. Num. Anal.,* **21,** 995–1011.

Thuburn, J., 1993: Use of a flux-limited scheme for vertical advection in a GCM. *Quart. J. Roy. Meteor Soc.* **119,** 469–487.

——, 1997: TVD schemes, positive schemes, and the universal limiter. *Mon. Wea. Rev.,* **125,** 1990–1993.

Tremback C. J., J. Powell, W. R. Cotton, and R. A. Pielke, 1987: The forward in time upstream advection scheme: Extension to higher orders. *Mon. Wea. Rev.,* **115,** 540–555.

van Leer, B., 1977: Toward the ultimate conservative difference scheme. IV: A new approach to numerical convection. *J. Comput. Phys.,* **23,** 276–299.

——, 1979: Toward the ultimate conservative difference scheme. V: A second order sequel to Godunov's method. *J. Comput. Phys.,* **32,** 101–136.

Xue, Y. K., and A. J. Thorpe, 1991: A mesoscale numerical model using the nonhydrostatic pressure-based sigma-coordinate equations: Model experiments with dry mountain flows. *Mon. Wea. Rev.,* **119,** 1168–1185.

Zalesak, S. T., 1979: Fully multidimensional flux-corrected transport algorithms for fluids. *J. Comput. Phys.,* **31,** 335–362.

——, 1987: A preliminary comparison of modern shock capturing schemes: Linear advection. *Adv. Compu. Methods Partial Diff. Equ. IMACS,* **VI,** 15–22.